

Analytical Large-Signal Modeling of Inverter-Based Microgrids With Koopman Operator Theory for Autonomous Control

Zixiao Ma¹, Member, IEEE, Zhaoyu Wang¹, Senior Member, IEEE, and Rui Cheng¹, Member, IEEE

Abstract—The microgrid (MG) plays a crucial role in the energy transition, but its nonlinearity presents a significant challenge for large-signal power systems studies in the electromagnetic transient (EMT) time scale. In this paper, we develop a large-signal linear MG model that considers the detailed dynamics of the primary and zero-control levels based on the Koopman operator (KO) theory. Firstly, a set of observable functions is carefully designed to capture the nonlinear dynamics of the MG. The corresponding linear KO is then analytically derived based on these observables, resulting in the linear representation of the original nonlinear MG with observables as the new coordinate. The influence of external input on the system dynamics is also considered during the derivation, enabling control of the MG. We solve the voltage control problem using the traditional linear quadratic integrator (LQI) method to demonstrate that textbook linear control techniques can accurately control the original nonlinear MG via the developed KO-linearized MG model. Our proposed KO linearization method is generic and can be easily extended for different control objectives and MG structures using our analytical derivation procedure. We validate the effectiveness of our methodology through various case studies.

Index Terms—Microgrid (MG), electromagnetic transient (EMT), Koopman operator (KO), large-signal modeling, microgrid voltage control.

I. INTRODUCTION

MICROGRIDS (MGs) are localized small-scale power systems with the integration of various distributed energy resources (DERs) such as solar panels, wind turbines, or generators to provide electricity to local consumers [1], [2], [3], [4], [5]. They are not only essential for enhancing the resilience, reliability, and efficiency of the power network, but also key to energy transition and decarbonization [6]. MGs can operate autonomously or be connected to the main grid. In grid-connected mode, the MG is mainly governed by the

main grid. While in islanded mode, local controls are needed to coordinate multiple DERs.

For simplifying the controller design, MG control is usually decoupled based on different time scales [1], [2]. Primary and zero-control levels stabilize the DERs at the fastest and lowest layer. The secondary control eliminates the steady-state error caused by the droop characteristics. The tertiary control focuses on economic dispatching and operation scheduling in the slowest time scale. For the secondary control level, there are two major approaches. One assumes that the zero-control level can always guarantee stability and provide fast and accurate reference tracking performance so that its dynamic model can be reduced [7]. This approach significantly increases the scalability of secondary control and enables large-scale system analysis. However, it inevitably results in the loss of the faster electromagnetic transient (EMT) [8], [9]. Moreover, large disturbances such as data loss, outliers, time delays, etc. are possible to happen in the feedback channel or actuator and result in an inappropriate secondary control signal that finally deteriorates the stability of the MG [10]. Therefore, another approach is to design the secondary controller with consideration of detailed dynamics of primary and zero-control levels in the EMT time scale [11], [12]. Such an approach can capture faster dynamics and yield a more reliable control strategy, nonetheless, the consideration of these dynamics considerably increases the system order as well as complexifies the nonlinearity of MGs [12].

Control of inverter-based MGs based on a nonlinear EMT model has been widely studied over the past decade [11], [12], [13]. However, controller design for nonlinear systems is usually case-by-case and can hardly be generalized to cope with different situations, such as time-delays [10], uncertainties [14], [15], constraints [16], etc. Thus, some studies sort to small-signal MG models based on linearization around an equilibrium point [8], [9]. With these models, one can use spectral tools to easily analyze the linear dynamics of MGs and adopt textbook linear control techniques to achieve various control objectives [17]. However, the results obtained with small-signal models are only valid within a neighborhood around the selected equilibrium.

Recently, the Koopman operator (KO) prevails as an effective linearization method that can accurately capture large-signal nonlinear dynamics. The essential idea is that a nonlinear dynamical system can be represented by an infinite-dimensional *linear* operator on a Hilbert space of

Manuscript received 22 March 2023; revised 7 August 2023; accepted 9 September 2023. This work was supported in part by the U.S. Department of Energy Wind Energy Technologies Office under Grant DE-EE0008956, and in part by the National Science Foundation under Grant ECCS 1929975 and Grant SBE 2228620. Paper no. TSG-00408-2023. (Corresponding author: Zhaoyu Wang.)

The authors are with the Department of Electrical and Computer Engineering, Iowa State University, Ames, IA 50011 USA (e-mail: zma@iastate.edu; wzy@iastate.edu; ruicheng@iastate.edu).

Color versions of one or more figures in this article are available at <https://doi.org/10.1109/TSG.2023.3314749>.

Digital Object Identifier 10.1109/TSG.2023.3314749

AQ1

vector-valued observable functions of system states [18]. The existing KO identification approaches can be classified into numerical (data-driven) and analytical (model-based) ones [19]. In *numerical* methods, a finite set of observable functions will be firstly designed based on the knowledge of dynamical system nonlinearity. Then, the KO will be identified using the system state's measurement data pairs of snapshots as it evolves in time. Representative methods include dynamic mode decomposition (DMD) [20], [21] and its extensions, such as extended DMD (EDMD) [22], and extended DMD with control (EDMDc) [23], etc. Especially from the MG control perspective, the KO is applied to the secondary control problem of MG in [24], [25]. Five observable functions are initiated and the KO is estimated by the EDMDc method with the assumption that the droop gains are known by the secondary controller. The assumption on the knowledge of local controllers is further relaxed and an enhanced observer Kalman filter to optimally identify the Koopman operator is proposed in [26]. The proposed approaches well fit the studied two-dimensional state-space model, nonetheless, they cannot capture the faster dynamics in the EMT time scale since the zero-control level is not considered. There are two major challenges to extending such numerical methods to the MGs modeled with EMT: firstly, to capture the EMT dynamics, model-free data-driven methods require measurements of the lower control levels, nonetheless, these measurements are usually not available due to limited meters; secondly, the dynamics of the lower control level significantly lift the observable space, such that an *exponentially increased volume of data pairs* are required for the numerical methods to produce an accurate estimation of the KO.

Another way to apply KO theory to *high-order nonlinear systems* is to use *analytical* methods that rely on the choice of observable functions [27]. If the observable functions are chosen perfectly, the nonlinear system can be represented in the lifted Hilbert space without any error. However, this is usually unachievable for most practical systems. A common strategy is to start with a set of observable functions and then expand them until the error between the nonlinear model and the KO linear model is sufficiently small [28]. Analytical methods provide an explicit linear model that does not need to be re-identified for different system settings as in numerical methods. However, deriving the KO analytically usually depends on the specific nonlinear dynamics of a practical system. For instance, [28] studied a nonlinear attitude control problem using the KO and selected the observables as the first n th-order derivatives of attitude dynamics. In [29], the KO was used to generate approximate analytical solutions for the motion of a satellite orbiting a non-spherical celestial body with zonal harmonics. It showed that the KO could capture any order of zonal harmonics without changing the methodology. To our best knowledge, no existing study has applied an analytical KO derivation method to MG control problems.

This paper proposes an analytical KO-based large-signal model linearization approach for inverter-dominated islanded MGs. The approach considers the detailed dynamics of primary and zero-control levels in the EMT time scale. To capture the nonlinear dynamics of the MG, we design a set of observables meticulously. Then, a KO is derived analytically

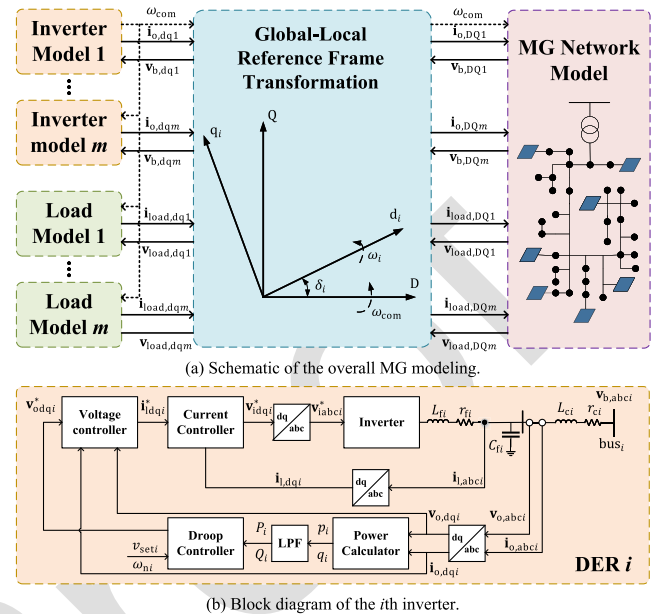


Fig. 1. Overall diagram of a nonlinear MG system model.

to represent the original nonlinear MG linearly with these observables as the new coordinate. To demonstrate that standard linear techniques are conveniently applicable, we solve the voltage control problem using the conventional linear quadratic integrator (LQI) method as an example. The main contributions of this paper are summarized as follows:

- A novel linear EMT MG model considering dynamics of primary and zero-control levels is proposed based on the KO theory that represents the nonlinear MG linearly with a finite set of tailored observable functions.
- Analytically derived KO is utilized to capture the nonlinear dynamics of the MG, thereby avoiding the need for huge data sets required by numerical approaches for high-dimensional complex nonlinear systems. Furthermore, the proposed KO-based model can be smoothly embedded into sophisticated linear control schemes.
- The proposed analytical KO-based model linearization methodology is generic and can be extended to other MGs with different control structures and topologies.

II. PRELIMINARIES

This section introduces a widely-used nonlinear MG model that forms the foundation for deriving the KO-linearized model in Section III. Additionally, the KO theory is briefly presented, with a focus on external control inputs that facilitate the use of linear control techniques.

A. MG Modeling

This section introduces the detailed nonlinear mathematical model of an MG based on [8]. Figure 1 shows the schematic of the overall MG model that is operating in the islanded mode. The mathematical models are derived for each component of the MG in the following subsections.

1) *Power Calculation and Droop Control*: The active and reactive power produced by the system can be determined by analyzing the transformed output voltage, v_{odq} , and current,

173 i_{odq} . To obtain the filtered instantaneous powers, a low-pass
174 filter with a corner frequency of ω_c can be utilized, which
175 yields the following results:

$$176 \quad \dot{P}_i = -P_i\omega_{ci} + \omega_{ci}(v_{odi}i_{odi} + v_{oqi}i_{oqi}), \quad (1a)$$

$$177 \quad \dot{Q}_i = -Q_i\omega_{ci} + \omega_{ci}(v_{oqi}i_{odi} - v_{odi}i_{oqi}). \quad (1b)$$

178 When operating in islanded mode, a DER lacks reference
179 inputs from the main grid, necessitating the use of droop con-
180 trollers to generate its own voltage and frequency references.
181 The process can be achieved through the following steps:

$$182 \quad \omega_i = \omega_n - D_{P_i}P_i, \quad (2a)$$

$$183 \quad v_{odi}^* = v_{seti} - D_{Q_i}Q_i, \quad (2b)$$

$$184 \quad v_{oqi}^* = 0. \quad (2c)$$

185 where ω_n and v_{seti} are nominal frequency and voltage set-
186 points, respectively. The detailed determination of droop gains
187 D_{P_i} and D_{Q_i} can be found in [8], [12].

188 2) *Voltage and Current Controllers*: The DER output volt-
189 ages and inductor currents are usually controlled via the
190 standard proportional–integral (PI) method at the zero level.
191 As shown below, the voltage controllers are designed to reg-
192 ulate the DER output voltages to their references which are
193 generated by the droop control at the primary level:

$$194 \quad \dot{\phi}_{di} = v_{odi}^* - v_{odi}, \quad (3a)$$

$$195 \quad \dot{i}_{ldi}^* = K_{ivi}\phi_{di} + K_{pvi}\dot{\phi}_{di} + F_i i_{od} - \omega_n C_{fi} v_{oqi}, \quad (3b)$$

$$196 \quad \dot{\phi}_{qi} = v_{oqi}^* - v_{oqi}, \quad (3c)$$

$$197 \quad \dot{i}_{lqi}^* = K_{ivi}\phi_{qi} + K_{pvi}\dot{\phi}_{qi} + F_i i_{oq} + \omega_n C_{fi} v_{od}. \quad (3d)$$

198 The commanded voltage reference, v_{ldqi}^* , is generated by
199 the current controllers through the computation of the error
200 between the reference inductor currents, i_{ldqi}^* , and correspond-
201 ing feedback measurements, i_{ldqi} :

$$202 \quad \dot{\gamma}_{di} = i_{ldi}^* - i_{ldi}, \quad (4a)$$

$$203 \quad v_{idi}^* = -\omega_n L_{fi} i_{lqi} + K_{ici}\gamma_{di} + K_{pci}\dot{\gamma}_{di}, \quad (4b)$$

$$204 \quad \dot{\gamma}_{qi} = i_{lqi}^* - i_{lqi}, \quad (4c)$$

$$205 \quad v_{iqi}^* = \omega_n L_{fi} i_{ldi} + K_{ici}\gamma_{qi} + K_{pci}\dot{\gamma}_{qi}. \quad (4d)$$

206 3) *LC Filters and Coupling Inductors*: By assuming that
207 the inverter produces the demanded voltage, i.e., $v_{idi} = v_{idi}^*$,
208 $v_{iqi} = v_{iqi}^*$, the dynamical models of LC filters and coupling
209 inductors are as follows

$$210 \quad \dot{i}_{ldi} = (-r_{fi}i_{ldi} + v_{idi} - v_{odi})/L_{fi} + \omega_i i_{lqi}, \quad (5a)$$

$$211 \quad \dot{i}_{lqi} = (-r_{fi}i_{lqi} + v_{iqi} - v_{oqi})/L_{fi} - \omega_i i_{ldi}, \quad (5b)$$

$$212 \quad \dot{v}_{odi} = (i_{ldi} - i_{odi})/C_{fi} + \omega_i v_{oqi}, \quad (5c)$$

$$213 \quad \dot{v}_{oqi} = (i_{lqi} - i_{oqi})/C_{fi} - \omega_i v_{odi}. \quad (5d)$$

$$214 \quad \dot{i}_{odi} = (-r_{ci}i_{odi} + v_{odi} - v_{bdi})/L_{ci} + \omega_i i_{oqi}, \quad (5e)$$

$$215 \quad \dot{i}_{oqi} = (-r_{ci}i_{oqi} + v_{oqi} - v_{bqi})/L_{ci} - \omega_i i_{odi}, \quad (5f)$$

216 4) *Transforming Local Reference Frame to Global Frame*:
217 The above mathematical model of each DER is developed in
218 their own local $d - q$ reference frame. Suppose that the local
219 $d - q$ reference frame of the i th DER is rotating at ω_i and the
220 global $D - Q$ reference frame is rotating at ω_{com} . Then, we
221 can connect each individual DER to the network by using the
222 following rotation transformation:

$$\begin{bmatrix} x_{Di} \\ x_{Qi} \end{bmatrix} = \begin{bmatrix} \cos \delta_i & -\sin \delta_i \\ \sin \delta_i & \cos \delta_i \end{bmatrix} \begin{bmatrix} x_{di} \\ x_{qi} \end{bmatrix} \quad (6) \quad 223$$

where x generally represents each state variable in (1)-(5), δ_i 224
is the difference between the global reference phase and the 225
local one of the i th DER, which is defined as 226

$$\dot{\delta}_i = \omega_i - \omega_{com} \quad (7) \quad 227$$

For islanded MGS, the first DER is selected as the common 228
global reference in the following derivation, i.e., $\omega_{com} = \omega_1$. 229

5) *Network Model*: The network model is developed in the 230
global reference frame. The dynamic model of the i th ($i =$ 231
 $1, \dots, q$) line current between bus j and bus k is represented 232
as follows, 233

$$\dot{i}_{linei} = (v_{bDj} - v_{bDk} - r_{linei}i_{linei})/L_{linei} + \omega_i i_{lineQi}, \quad (8a) \quad 234$$

$$\dot{i}_{linei} = (v_{bQj} - v_{bQk} - r_{linei}i_{linei})/L_{linei} - \omega_i i_{lineDi}. \quad (8b) \quad 235$$

6) *Load Model*: As in [8], purely resistive loads and 236
resistors and inductors (RL loads) are considered. The purely 237
resistive loads directly follow Ohm's law without dynamics. 238
While the i th ($i = 1, \dots, p$) RL load can be modeled as, 239

$$\dot{i}_{loadDi} = (v_{bDi} - R_{loadi}i_{loadDi})/L_{loadi} + \omega_i i_{loadQi}, \quad (9a) \quad 240$$

$$\dot{i}_{loadQi} = (v_{bQi} - R_{loadi}i_{loadQi})/L_{loadi} - \omega_i i_{loadDi}. \quad (9b) \quad 241$$

The frequency is constant throughout the network, thus the 242
dynamic equations of lines and loads can adopt ω_1 derived 243
from the first inverter [9]. 244

7) *Virtual Resistor Method*: As shown in (5), (8) and (9), 245
the bus voltages are treated as inputs to each subsystem, such 246
that the influences of load perturbation could not be precisely 247
predicted [9]. To define the bus voltage, a virtual resistor is 248
assumed between each bus and the ground. By selecting a suf- 249
ficiently large resistance r_n for the virtual resistor, its impact 250
on the system dynamics can be negligible. Then, the bus volt- 251
age connecting the inverters, loads and the network can be 252
defined as 253

$$v_{bDi} = r_n \left(i_{oDi} - i_{loadDi} + \sum_{j=1}^N i_{lineDi,j} \right), \quad (10a) \quad 254$$

$$v_{bQi} = r_n \left(i_{oQi} - i_{loadQi} + \sum_{j=1}^N i_{lineQi,j} \right) \quad (10b) \quad 255$$

where N is the number of lines connected to bus i . Care 256
should be taken on the direction of line currents in the last 257
term of (10). We assume the current entering the bus to be 258
positive and the current leaving the bus to be negative. 259

B. *Compact Nonlinear Model of an MG for Voltage Control* 260

For the ease of deriving KO for the MG system, we stack up 261
the state variables to form a compact state space model. From 262
the viewpoint of voltage control, an inverter-based islanded 263
MG with m DERs, p RL loads, and q lines can be represented 264
as follows: 265

$$\dot{\mathbf{x}}(t) = \mathbf{f}(\mathbf{x}(t), \mathbf{u}(t)), \quad (11) \quad 266$$

where $\mathbf{x} = [\mathbf{x}_{inv1}^\top, \dots, \mathbf{x}_{invm}^\top, \mathbf{x}_{line1}^\top, \dots, \mathbf{x}_{lineq}^\top,$ 267
 $\mathbf{x}_{load1}^\top, \dots, \mathbf{x}_{loadp}^\top]^\top$ is the state vector of 268

269 inverters, lines and loads; $\mathbf{x}_{invi} = [\delta_i, P_i, Q_i,$
 270 $\phi_{di}, \phi_{qi}, \gamma_{di}, \gamma_{qi}, i_{di}, i_{qi}, v_{odi}, v_{oqi}, i_{odi}, i_{oqi}]^\top, i = 1, \dots, m,$
 271 denotes the state variables of the i^{th} DER;
 272 $\mathbf{x}_{linei} = [i_{lineDi}, i_{lineQi}]^\top, i = 1, \dots, q,$ are the currents
 273 of the i^{th} line; $\mathbf{x}_{loadi} = [i_{loadDi}, i_{loadQi}]^\top, i = 1, \dots, p,$
 274 are the currents of the i^{th} load; $\mathbf{u} = [v_{set1}, \dots, v_{setm}]^\top$
 275 denotes the voltage control signal to be designed. Denoting
 276 $n = 13m + 2p + 2q, \mathbf{f}: \mathbb{R}^n \times \mathbb{R}^m \rightarrow \mathbb{R}^n$ is the state
 277 function describing the nonlinear system dynamics. This
 278 high-dimensional dynamic model represents the detailed
 279 transient dynamics of the whole MG in the EMT time scale,
 280 thus facilitating fast dynamical analysis and control.

281 C. Brief Introduction of Koopman Operator Theory

282 The MG system described in (11) comprehensively models
 283 the primary and zero-control levels, resulting in a high-
 284 dimensional nonlinear system. Despite the increasing impor-
 285 tance of stability analysis and controller design for dynamical
 286 systems, the system's nonlinearity presents a significant chal-
 287 lenge for comprehensive analysis. Traditional nonlinear control
 288 methods, in particular, exhibit low generality and require
 289 complex potential function designs. From a practical stand-
 290 point, it is crucial to develop an accurate large-signal linearized
 291 MG model that bridges existing mature linear control methods
 292 and the nonlinear MG system.

293 The KO theory has gained considerable attention in nonlin-
 294 ear control theory and application as an effective linearization
 295 method that can accurately capture large-signal nonlinear
 296 dynamics. The fundamental concept of KO theory is to repre-
 297 sent a nonlinear system as an infinite-dimensional linear oper-
 298 ator on a Hilbert space of vector-valued observable functions \mathbf{g}
 299 of system states. Recalling the MG system model (11), where
 300 \mathbf{x} and \mathbf{u} evolve on smooth manifolds \mathcal{M} and \mathcal{N} , respectively,
 301 we define the *observable vector* $\mathbf{z} = \mathbf{g}(\mathbf{x}, \mathbf{u}): \mathcal{M} \times \mathcal{N} \rightarrow \mathbb{R}^N$.
 302 Then, with an infinite-dimensional linear operator acting on
 303 the observable functions, the system dynamics of (11) can be
 304 described linearly in this Hilbert space, i.e.,

$$305 \quad \mathcal{K}\mathbf{g}(\mathbf{x}, \mathbf{u}) = \frac{d\mathbf{g}(\mathbf{x}, \mathbf{u})}{dt} = f_1 \frac{\partial \mathbf{g}}{\partial x_1} + \dots$$

$$306 \quad + f_n \frac{\partial \mathbf{g}}{\partial x_n} + \dot{u}_1 \frac{\partial \mathbf{g}}{\partial u_1} + \dots + \dot{u}_m \frac{\partial \mathbf{g}}{\partial u_m}. \quad (12)$$

307 where $\mathbf{x} = [x_1, \dots, x_n]$ and $\mathbf{u} = [u_1, \dots, u_m]$. In Eq. (12), we
 308 follow the assumption in [25] that the control signals influ-
 309 ence the state evolution, but they are not evolving dynamically,
 310 i.e., $\dot{\mathbf{u}} = \mathbf{0}$. The above equation (12) indicates that the KO
 311 intrinsically describes the dynamical evolution of the obser-
 312 vation of the state and input $\mathbf{g}(\mathbf{x}, \mathbf{u})$ in a linear manner as
 313 illustrated in Fig. 2. Therefore, it sheds light on analyzing
 314 the system dynamics with spectral methods and design con-
 315 trollers with the existing general linear control methodologies
 316 for nonlinear systems (11) in the KO-oriented linear space.

317 From a practical engineering perspective, it is important
 318 to note that an infinite-dimensional system is not feasible.
 319 Therefore, the key to utilizing KO theory lies in identify-
 320 ing an appropriate set of finite-dimensional observables and
 321 the corresponding KO that captures the primary dynamics
 322 in the Hilbert space. In the following section, we develop a

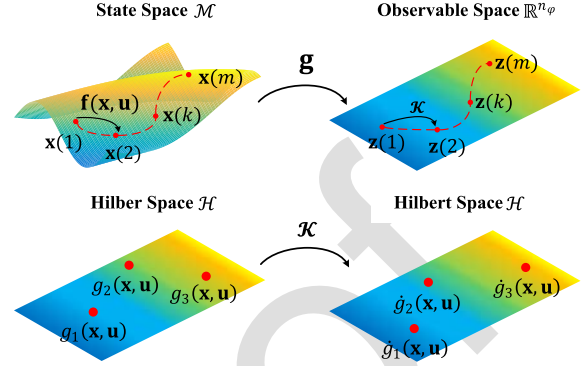


Fig. 2. Illustration of the KO theory. The upper row illustrates that a dynamic system can be measured by an infinite set of observable functions \mathbf{g} . The lower row explains that the KO, \mathcal{K} , describes the dynamical evolution of the observation of the state and input, $\mathbf{g}(\mathbf{x}, \mathbf{u})$, in a linear manner.

KO-linearized MG model with finite-dimensional observables 323
 using an analytical approach. 324

325 III. DERIVATION OF KO-LINEARIZED MG MODEL 325

326 In this section, we present an analytical method to develop 326
 a KO-linearized model of the MG system (11) in the EMT 327
 time-scale, which is proposed for the first time. The deriva- 328
 tion process involves several steps. First, assumptions are made 329
 to eliminate the nonlinearities that have negligible impact on 330
 the model accuracy. Second, we rearrange the elements in \mathbf{x} 331
 to separate the linear and nonlinear terms of the system (11). 332
 Third, the KO theory is applied to eliminate the nonlinear 333
 terms by designing and extending tailored observable func- 334
 tions. The selection of appropriate observable functions is 335
 crucial to ensure the stabilizability of the new linear system 336
 for MG voltage control. Finally, we present the KO-linearized 337
 model in a concise form. 338

339 A. Assumptions 339

340 To simplify the derivation, we make some reasonable 340
 assumptions: 1) Since DER 1 is chosen as the common global 341
 reference, the difference angle between its global and local 342
 reference frame is $\delta_1 = 0$ with a zero initial value based on 343
 Eq. (7). Therefore, around the equilibrium, δ_i are small and 344
 we can approximate that $\sin \delta_i \approx \delta_i$ and $\cos \delta_i \approx 1$; 2) Since 345
 the $P - \omega$ droop gain is minuscule, we assume $\omega_i \approx \omega_n$ only 346
 in the coupling inductor terms in LC filters (5) and line cur- 347
 rents (8). 3) More common resistive loads are considered in 348
 the following derivation to reduce the load dynamics. We rig- 349
 orously test the model error caused by these assumptions in 350
 Section V-C under different conditions. The result shows that 351
 these assumptions are valid and acceptable. 352

353 B. Separating Linear and Nonlinear Subsystems 353

354 Based on the above assumptions, some state variables 354
 exhibit linear dynamics with respect to the system state \mathbf{x} from 355
 Eq. (1) to Eq. (10). We simplify the derivation by directly 356
 extracting and incorporating these linear equations into the 357
 final KO-linearized model and addressing the remaining non- 358
 linear dynamics with the KO. 359

360 1) *Linear Subsystems*: Define state vector whose dynamics
361 linearly depends on \mathbf{x} as

$$362 \quad \mathbf{x}_{Li} = [\delta_i, \phi_{di}, \phi_{qi}, \gamma_{di}, \gamma_{qi}, i_{ldi}, i_{lqi}, v_{odi}, v_{oqi}]^\top, \quad (13)$$

$$363 \quad i = 2, \dots, m.$$

364 Since DER 1 is selected as the common reference, it has
365 $\sin \delta_1 = 0$, $\cos \delta_1 = 1$ with $\delta_1(0) = 0$. Then, for DER 1, the
366 nonlinearities caused by frame transformation (6) for v_{bd1} and
367 v_{bq1} are eliminated, such that (5e)-(5f) become linear equations
368 with $i = 1$, i.e.,

$$369 \quad \mathbf{x}_{L1} = [\phi_{d1}, \phi_{q1}, \gamma_{d1}, \gamma_{q1}, i_{ld1}, i_{lq1}, v_{od1}, v_{oq1}, i_{od1}, i_{oq1}]^\top. \quad (14)$$

370 The state-space model with respect to $\mathbf{x}_L = [\mathbf{x}_{L1}^\top, \dots, \mathbf{x}_{Lm}^\top]^\top$
371 is derived respectively as

$$372 \quad \dot{\mathbf{x}}_{L1} = \mathcal{A}_{inv1} \mathbf{x}_{L1} + \mathcal{A}_1 [Q_1, i_{lineD1}, i_{lineQ1}]^\top + \mathcal{B}_1 v_{set1}, \quad (15)$$

$$373 \quad \dot{\mathbf{x}}_{Li} = \mathcal{A}_{invi} \mathbf{x}_{Li} + \mathcal{A}_i [P_i, Q_i, i_{odi}, i_{oqi}]^\top + \mathcal{B}_i v_{seti} \quad (16)$$

374 where \mathcal{A}_{inv1} , \mathcal{A}_{invi} , \mathcal{A}_1 and \mathcal{A}_i are given in (17)-(20),
375 respectively and $\mathcal{B}_1 = [1, 0, K_{pv1}, 0, b_1, 0, 0, 0, 0]^\top$, $\mathcal{B}_i =$
376 $[0, 1, 0, K_{pvi}, 0, b_i, 0, 0, 0]^\top$ for $i = 2, \dots, m$; moreover

$$377 \quad a_{i,1} = \frac{K_{pci} K_{pvi} D_{Qi}}{L_{fi}}, a_{i,2} = \frac{K_{pci} K_{ivi}}{L_{fi}}, a_{i,3} = \frac{K_{ici}}{L_{fi}},$$

$$378 \quad a_{i,4} = \frac{r_{fi} + K_{pci}}{L_{fi}}, a_{i,5} = \frac{1 + K_{pvi} K_{pvi}}{L_{fi}}, a_{i,6} = \frac{K_{pci} \omega_n C_{fi}}{L_{fi}},$$

$$379 \quad a_{i,7} = \frac{K_{pci} F_i}{L_{fi}}, a_{i,8} = \frac{r_{ci}}{L_{ci}} + \frac{R_{loadi} r_n}{L_{ci}(r_n + R_{loadi})},$$

$$380 \quad a_{i,9} = \frac{R_{loadi} r_n}{L_{ci}(r_n + R_{loadi})}, b_i = \frac{K_{pvi} K_{pvi}}{L_{fi}}, \text{ for } i = 1, \dots, m.$$

$$381 \quad \mathcal{A}_{inv1} = \begin{bmatrix} 0 & 0 & 0 & 0 & 0 & 0 & -1 & 0 & 0 & 0 \\ 0 & 0 & 0 & 0 & 0 & 0 & 0 & -1 & 0 & 0 \\ K_{iv1} & 0 & 0 & 0 & -1 & 0 & -K_{pv1} & -\omega_n C_{f1} & F_1 & 0 \\ 0 & K_{iv1} & 0 & 0 & 0 & -1 & \omega_n C_{f1} & -K_{pv1} & 0 & F_1 \\ a_{1,2} & 0 & a_{1,3} & 0 & -a_{1,4} & 0 & -a_{1,5} & -a_{1,6} & a_{1,7} & 0 \\ 0 & a_{1,2} & 0 & a_{1,3} & 0 & -a_{1,4} & a_{1,6} & -a_{1,5} & 0 & a_{1,7} \\ 0 & 0 & 0 & 0 & 0 & \frac{1}{C_{f1}} & 0 & 0 & \omega_n & -\frac{1}{C_{f1}} \\ 0 & 0 & 0 & 0 & 0 & 0 & \frac{1}{C_{f1}} & -\omega_n & 0 & 0 \\ 0 & 0 & 0 & 0 & 0 & 0 & 0 & \frac{1}{L_{c1}} & 0 & -a_{1,8} \\ 0 & 0 & 0 & 0 & 0 & 0 & 0 & \frac{1}{L_{c1}} & -\omega_n & -a_{1,8} \end{bmatrix} \quad (17)$$

$$382 \quad \mathcal{A}_{invi} = \begin{bmatrix} 0 & 0 & 0 & 0 & 0 & 0 & 0 & 0 & 0 & 0 \\ 0 & 0 & 0 & 0 & 0 & 0 & 0 & -1 & 0 & 0 \\ 0 & 0 & 0 & 0 & 0 & 0 & 0 & 0 & -1 & 0 \\ 0 & K_{ivi} & 0 & 0 & 0 & -1 & 0 & -K_{pvi} & -\omega_n C_{fi} & 0 \\ 0 & 0 & K_{ivi} & 0 & 0 & 0 & -1 & \omega_n C_{fi} & -K_{pvi} & 0 \\ 0 & a_{i,2} & 0 & a_{i,3} & 0 & -a_{i,4} & 0 & -a_{i,5} & -a_{i,6} & 0 \\ 0 & 0 & a_{i,2} & 0 & a_{i,3} & 0 & -a_{i,4} & a_{i,6} & -a_{i,5} & 0 \\ 0 & 0 & 0 & 0 & 0 & 0 & \frac{1}{C_{fi}} & 0 & 0 & \omega_n \\ 0 & 0 & 0 & 0 & 0 & 0 & 0 & \frac{1}{C_{fi}} & -\omega_n & 0 \end{bmatrix} \quad (18)$$

$$383 \quad \mathcal{A}_1 = \begin{bmatrix} -D_{Q1} & 0 & 0 \\ 0 & 0 & 0 \\ -K_{pv1} D_{Q1} & 0 & 0 \\ 0 & 0 & 0 \\ -a_{1,1} & 0 & 0 \\ 0 & 0 & 0 \\ 0 & 0 & 0 \\ 0 & 0 & 0 \\ 0 & a_{1,9} & 0 \\ 0 & 0 & -a_{1,9} \end{bmatrix} \quad (19)$$

$$384 \quad \mathcal{A}_i = \begin{bmatrix} D_{Pi} & -D_{Pi} & 0 & 0 & 0 \\ 0 & 0 & -D_{Qi} & 0 & 0 \\ 0 & 0 & 0 & 0 & 0 \\ 0 & 0 & -K_{pvi} D_{Qi} & F_i & 0 \\ 0 & 0 & 0 & 0 & F_i \\ 0 & 0 & -a_{i,1} & a_{i,7} & 0 \\ 0 & 0 & 0 & 0 & a_{i,7} \\ 0 & 0 & 0 & -\frac{1}{C_{fi}} & 0 \\ 0 & 0 & 0 & 0 & -\frac{1}{C_{fi}} \end{bmatrix} \quad (20)$$

386 2) *Nonlinear Subsystems (DER Output Power)*: We rewrite
387 the dynamics of active and reactive powers (1) as

$$388 \quad \underbrace{\begin{bmatrix} \dot{P}_i \\ \dot{Q}_i \end{bmatrix}}_{\dot{\mathbf{x}}_{pqi}} = - \underbrace{\begin{bmatrix} \omega_{ci} & 0 \\ 0 & \omega_{ci} \end{bmatrix}}_{\mathbf{W}_{ci}} \underbrace{\begin{bmatrix} P_i \\ Q_i \end{bmatrix}}_{\mathbf{x}_{pqi}} + \underbrace{\begin{bmatrix} \omega_{ci} & 0 \\ 0 & \omega_{ci} \end{bmatrix}}_{\mathbf{W}_{ci}} \underbrace{\begin{bmatrix} v_{odi} & v_{oqi} \\ v_{oqi} & -v_{odi} \end{bmatrix}}_{\mathbf{V}_{oi}} \underbrace{\begin{bmatrix} i_{odi} \\ i_{oqi} \end{bmatrix}}_{\mathbf{I}_{oi}} \triangleq \underbrace{\begin{bmatrix} z_{i,1} \\ z_{i,2} \end{bmatrix}}_{\mathbf{z}_{i,1}}. \quad (21)$$

390 In (21), $\mathbf{z}_{i,1}$ is a designed observable vector. For the control
391 perspective, we take the second derivative of $\mathbf{z}_{i,1}$ until the control
392 signal \mathbf{u} appears in the second derivative of DER output
393 voltage \ddot{v}_{odi} . The derivation process is as follows,

$$394 \quad \dot{\mathbf{z}}_{i,1} = -\mathbf{W}_{ci} \mathbf{z}_{i,1} + \mathbf{W}_{ci} (\dot{\mathbf{V}}_{oi} \mathbf{I}_{oi} + \dot{\mathbf{V}}_{oi} \dot{\mathbf{I}}_{oi}) \triangleq \mathbf{z}_{i,2}, \quad (22)$$

$$395 \quad \dot{\mathbf{z}}_{i,2} = -\mathbf{W}_{ci} \mathbf{z}_{i,2} + \mathbf{W}_{ci} (\ddot{\mathbf{V}}_{oi} \mathbf{I}_{oi} + 2\dot{\mathbf{V}}_{oi} \dot{\mathbf{I}}_{oi} + \mathbf{V}_{oi} \ddot{\mathbf{I}}_{oi}). \quad (23)$$

396 Define the second term at the right-hand side of (23) as \mathbf{U}_{pqi} :

$$397 \quad \mathbf{U}_{pqi} = \mathbf{W}_{ci} (\ddot{\mathbf{V}}_{oi} \mathbf{I}_{oi} + 2\dot{\mathbf{V}}_{oi} \dot{\mathbf{I}}_{oi} + \mathbf{V}_{oi} \ddot{\mathbf{I}}_{oi})$$

$$398 \quad = \mathbf{W}_{ci} \left(\begin{bmatrix} \ddot{v}_{oqi} i_{oqi} \\ \ddot{v}_{oqi} i_{odi} \end{bmatrix} + 2\dot{\mathbf{V}}_{oi} \dot{\mathbf{I}}_{oi} + \mathbf{V}_{oi} \ddot{\mathbf{I}}_{oi} + \begin{bmatrix} \ddot{v}_{odi} i_{odi} \\ -\ddot{v}_{odi} i_{oqi} \end{bmatrix} \right)$$

$$399 \quad \triangleq \mathbf{f}_{pqi}(\mathbf{x}) + \mathcal{B}_{pqi} \mathbf{u} \quad (24)$$

400 where $\mathbf{f}_{pqi}(\mathbf{x})$ is a nonlinear vector-valued function of \mathbf{x} that
401 can be extracted by subtracting $\mathcal{B}_{pqi} \mathbf{u}$ from \mathbf{U}_{pqi} and

$$402 \quad \mathcal{B}_{pqi} = \begin{bmatrix} \frac{b_i \omega_{ci} i_{odi}}{C_{fi}} & 0 & 0 \\ -\frac{b_i \omega_{ci} i_{oqi}}{C_{fi}} & 0 & 0 \end{bmatrix} \quad (25)$$

403 In conclusion, we define the observable vector for the
404 nonlinear subsystems with respect to DER output power as

$$405 \quad \mathbf{z}_{pqi} = [\mathbf{x}_{pqi}^\top, \mathbf{z}_{i,1}^\top, \mathbf{z}_{i,2}^\top]^\top, \quad i = 1, \dots, m.$$

406 3) *Nonlinear Subsystems (Currents of DERs and Network)*:
407 Since the DER output currents are coupled with the network
408 currents, we handle them together and define

$$409 \quad \mathbf{x}_{net} = [i_{odi}, i_{oqi}, i_{lineDj}, i_{lineQj}]^\top,$$

$$410 \quad i = 2, \dots, m, \quad j = 1, \dots, q. \quad (26)$$

411 Then, from (5e)-(10), we rewrite the state equations as

$$412 \quad \dot{\mathbf{x}}_{net} = \mathcal{A}_{net} \mathbf{x}_{net} + \mathbf{H} \xi + \mathbf{D} \mathbf{x}_{net} \triangleq \mathbf{z}_{net1}, \quad (27)$$

413 The positions of elements in \mathcal{A}_{net} , \mathbf{H} , and \mathbf{D} depend on the
414 topology of the MG. To illustrate the derivation, we take a
415 test system shown in Fig. 3 as an example. Then, $\mathbf{x}_{net} =$
416 $[i_{od2}, i_{oq2}, i_{od3}, i_{oq3}, i_{lineD1}, i_{lineQ1}, i_{lineD2}, i_{lineQ2}]^\top$, $\xi = [i_{od1},$

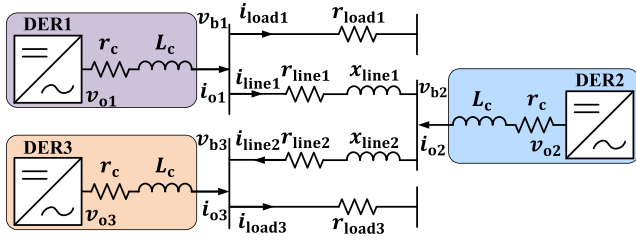


Fig. 3. Diagram of the test MG system.

417 $[i_{oq1}, v_{od2}, v_{oq2}, v_{od3}, v_{oq3}]^T$ and the matrices are given as
418 follows,

$$419 \mathbf{A}_{\text{net}} = \begin{bmatrix} -a_{2,8} & \omega_n & 0 & 0 & -a_{2,9} & 0 & a_{2,9} & 0 \\ -\omega_n & -a_{2,8} & 0 & 0 & 0 & a_{2,9} & 0 & -a_{2,9} \\ 0 & 0 & -a_{3,8} & \omega_n & 0 & 0 & -a_{3,9} & 0 \\ 0 & 0 & -\omega_n & -a_{3,8} & 0 & 0 & 0 & a_{3,9} \\ -\frac{r_n}{L_{\text{line1}}} & 0 & 0 & 0 & -a_{10} & \omega_n & \frac{r_n}{L_{\text{line1}}} & 0 \\ -\frac{r_n}{L_{\text{line1}}} & 0 & 0 & 0 & -\omega_n & -a_{10} & 0 & \frac{r_n}{L_{\text{line1}}} \\ \frac{r_n}{L_{\text{line2}}} & 0 & -a_{13} & 0 & \frac{r_n}{L_{\text{line2}}} & 0 & -a_{11} & \omega_n \\ 0 & \frac{r_n}{L_{\text{line2}}} & 0 & -a_{13} & 0 & \frac{r_n}{L_{\text{line2}}} & -\omega_n & -a_{11} \end{bmatrix} \quad (28)$$

$$421 \mathbf{H} = \begin{bmatrix} 0 & 0 & \frac{1}{L_{c2}} & 0 & 0 & 0 \\ 0 & 0 & 0 & \frac{1}{L_{c2}} & 0 & 0 \\ 0 & 0 & 0 & 0 & \frac{1}{L_{c3}} & 0 \\ 0 & 0 & 0 & 0 & 0 & \frac{1}{L_{c3}} \\ a_{12} & 0 & 0 & 0 & 0 & 0 \\ 0 & a_{12} & 0 & 0 & 0 & 0 \\ 0 & 0 & 0 & 0 & 0 & 0 \\ 0 & 0 & 0 & 0 & 0 & 0 \end{bmatrix} \quad (29)$$

$$422 \mathbf{D} = \begin{bmatrix} 0 & 0 & 0 & 0 & 0 & -a_{2,9}\delta_2 & 0 & a_{2,9}\delta_2 \\ 0 & 0 & 0 & 0 & a_{2,9}\delta_2 & 0 & -a_{2,9}\delta_2 & 0 \\ 0 & 0 & 0 & 0 & 0 & 0 & 0 & -a_{3,9}\delta_3 \\ 0 & 0 & 0 & 0 & 0 & 0 & a_{3,9}\delta_3 & 0 \\ 0 & \frac{r_n\delta_2}{L_{\text{line1}}} & 0 & 0 & 0 & 0 & 0 & 0 \\ -\frac{r_n\delta_2}{L_{\text{line1}}} & 0 & 0 & 0 & 0 & 0 & 0 & 0 \\ 0 & -\frac{r_n\delta_2}{L_{\text{line2}}} & 0 & a_{13}\delta_3 & 0 & 0 & 0 & 0 \\ \frac{r_n\delta_2}{L_{\text{line2}}} & 0 & -a_{13}\delta_3 & 0 & 0 & 0 & 0 & 0 \end{bmatrix} \quad (30)$$

424 where the parameters a_{10} to a_{13} are defined as

$$425 a_{10} = \frac{r_{\text{line1}} + r_n}{L_{\text{line1}}} + \frac{R_{\text{load1}}r_n}{L_{\text{line1}}(R_{\text{load1}} + r_n)},$$

$$426 a_{11} = \frac{r_{\text{line2}} + r_n}{L_{\text{line2}}} + \frac{R_{\text{load3}}r_n}{L_{\text{line2}}(R_{\text{load3}} + r_n)},$$

$$427 a_{12} = \frac{R_{\text{load1}}r_n}{L_{\text{line1}}(R_{\text{load1}} + r_n)}, a_{13} = \frac{R_{\text{load3}}r_n}{L_{\text{line2}}(R_{\text{load3}} + r_n)}$$

428 For the control purpose, we take the second derivative of
429 \mathbf{z}_{net1} until the control signal \mathbf{u} appears in the second derivative
430 of \ddot{v}_{odi} in $\ddot{\xi}$. The derivation process is as follows,

$$431 \dot{\mathbf{z}}_{\text{net1}} = \mathbf{A}_{\text{net}}\mathbf{z}_{\text{net1}} + \mathbf{H}\dot{\xi} + \dot{\mathbf{D}}\mathbf{x}_{\text{net}} + \mathbf{D}\mathbf{z}_{\text{net1}} \triangleq \mathbf{z}_{\text{net2}}, \quad (31)$$

$$432 \dot{\mathbf{z}}_{\text{net2}} = \mathbf{A}_{\text{net}}\mathbf{z}_{\text{net2}} + \ddot{\mathbf{D}}\mathbf{x}_{\text{net}} + 2\dot{\mathbf{D}}\mathbf{z}_{\text{net1}} + \mathbf{D}\mathbf{z}_{\text{net2}} + \mathbf{H}\ddot{\xi}. \quad (32)$$

433 Define the control vector \mathbf{U}_{net} as (33). Note that \mathbf{z}_{net1} and \mathbf{z}_{net2}
434 can be represented with \mathbf{x} , and \mathbf{u} can be extracted from $\ddot{\xi}$, thus

the control vector \mathbf{U}_{net} can be separated as follows,

$$435 \mathbf{U}_{\text{net}} = \ddot{\mathbf{D}}\mathbf{x}_{\text{net}} + 2\dot{\mathbf{D}}\mathbf{z}_{\text{net1}} + \mathbf{D}\mathbf{z}_{\text{net2}} + \mathbf{H}\ddot{\xi} \quad 436$$

$$437 = \underbrace{\ddot{\mathbf{D}}\mathbf{x}_{\text{net}} + 2\dot{\mathbf{D}}\mathbf{z}_{\text{net1}} + \mathbf{D}\mathbf{z}_{\text{net2}} + \mathbf{H}\ddot{\xi}^*}_{\mathbf{f}_{\text{net}}(\mathbf{x})} + \mathcal{B}_{\text{net}}\mathbf{u} \quad (33) \quad 437$$

438 where $\ddot{\xi}^* = \ddot{\xi} - \mathcal{B}_{\text{net}}\mathbf{u}$, $\mathcal{B}_{\text{net}} = \mathbf{H}\bar{\mathcal{B}}_{\text{net}}$ and

$$439 \bar{\mathcal{B}}_{\text{net}} = \begin{bmatrix} 0 & 0 & 0 \\ 0 & 0 & 0 \\ 0 & b_2 & 0 \\ 0 & 0 & 0 \\ 0 & 0 & b_3 \\ 0 & 0 & 0 \end{bmatrix} \quad (34) \quad 439$$

440 In conclusion, we define the observable vector for the nonlinear
441 subsystems with respect to DER output currents and the
442 network as

$$443 \mathbf{z}_{\text{net}} = [\mathbf{x}_{\text{net}}^T, \mathbf{z}_{\text{net1}}^T, \mathbf{z}_{\text{net2}}^T]^T. \quad (35) \quad 443$$

444 *Remark 1:* The treatment in the KO derivations (21)-
445 (24) and (27)-(33) embodies a comparable concept to that
446 of input-state feedback linearization. However, their intrinsic
447 philosophies diverge significantly. Primarily, input-state feed-
448 back linearization endeavors to eliminate all nonlinearities in
449 the state space by determining appropriate changes in state
450 variables and employing feedback control laws. This process
451 remains confined to the state space and typically does not
452 result in an increase in state or input dimensions. Conversely,
453 the proposed analytical method linearly represents the non-
454 linear MG system in a lifted observable space and control
455 input space, which constitutes the fundamental characteristic
456 of KO. Secondly, while input-state feedback can yield a per-
457 fectly linear model, achieving input-state feedback lineariza-
458 tion necessitates meeting a series of feedback-linearizable
459 conditions to guarantee the existence of a solution. These
460 feedback-linearizable conditions (e.g., [30, Th. 13.2]) may not
461 be applicable to MG and can be difficult to verify for high-
462 order nonlinear systems. In contrast, the KO-based method
463 can consistently furnish an approximated (or ideally, a per-
464 fect, contingent upon the impeccable selection of observables
465 or infinite-dimensional considerations) linear model. Finally,
466 due to the fundamentally distinct overall derivation philosophy,
467 the final KO-linearized model (36) deviates from Brunovsky's
468 canonical form as seen in feedback linearization.

469 C. Overall KO-Linearized MG Model

470 Defining the observable vector of the overall MG system
471 as $\mathbf{z} = [\mathbf{x}_{\text{L}}^T, \mathbf{z}_{\text{pq1}}^T, \dots, \mathbf{z}_{\text{pqm}}^T, \mathbf{z}_{\text{net}}^T]^T \in \mathbb{R}^N$, the KO-linearized
472 model can be concluded as

$$473 \dot{\mathbf{z}} = \mathbf{A}\mathbf{z} + \mathbf{B}\mathbf{U}, \quad (36a) \quad 473$$

$$474 \mathbf{y} = \mathbf{C}\mathbf{z} \quad (36b) \quad 474$$

475 where $\mathbf{y} = [v_{od1}, \dots, v_{odm}]^T \in \mathbb{R}^M$ is the output vector, which
476 can be extracted from the state vector with matrix \mathbf{C} , $\mathbf{U} =$
477 $[\mathbf{u}^T, \mathbf{U}_{\text{pq1}}^T, \dots, \mathbf{U}_{\text{pqm}}^T, \mathbf{U}_{\text{net}}^T]^T$ is the lifted control input vector to
478 be designed according to the control performance requirement.

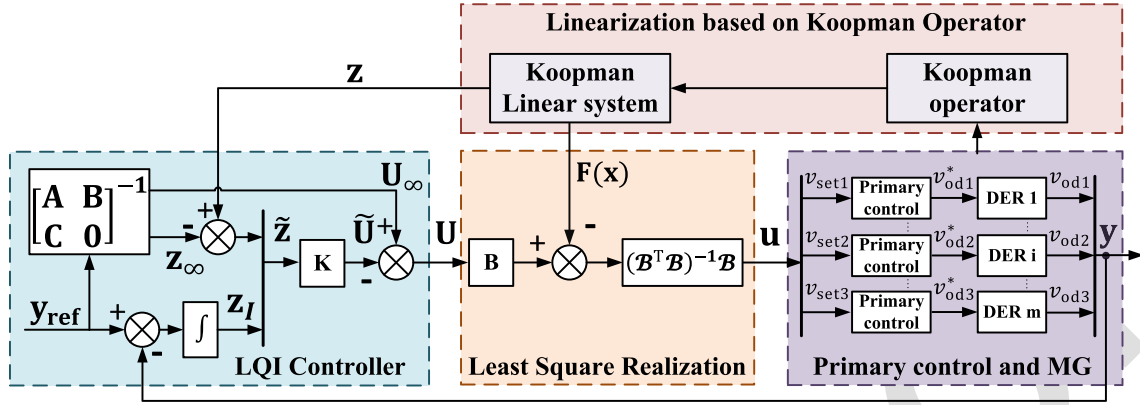


Fig. 4. Closed-loop MG control system based on the KO-linearized model and LQI. The LQI gain is $\mathbf{K} = \mathbf{R}^{-1} \tilde{\mathbf{B}}^T \mathbf{P}$.

Take the system in Fig. 3 as an example, $m = 3$ and $N = 70$. Then the corresponding matrices \mathbf{A} and \mathbf{B} are derived as below

$$\mathbf{A} = \begin{bmatrix} \mathcal{A}_{\text{inv}1} & \mathbf{0} & \mathbf{0} & \mathcal{A}_1^1 & \mathbf{0} & \mathbf{0} & \mathcal{A}_1^{2,3} & \mathbf{0} & \mathbf{0} \\ \mathbf{0} & \mathcal{A}_{\text{inv}2} & \mathbf{0} & \mathcal{A}_2^1 & \mathcal{A}_2^{2,3} & \mathbf{0} & \mathcal{A}_2^{4,5} & \mathbf{0} & \mathbf{0} \\ \mathbf{0} & \mathbf{0} & \mathcal{A}_{\text{inv}3} & \mathcal{A}_3^1 & \mathbf{0} & \mathcal{A}_3^{2,3} & \mathcal{A}_3^{4,5} & \mathbf{0} & \mathbf{0} \\ \mathbf{0} & \mathbf{0} & \mathbf{0} & \mathcal{A}_{\omega_1} & \mathbf{0} & \mathbf{0} & \mathbf{0} & \mathbf{0} & \mathbf{0} \\ \mathbf{0} & \mathbf{0} & \mathbf{0} & \mathbf{0} & \mathcal{A}_{\omega_2} & \mathbf{0} & \mathbf{0} & \mathbf{0} & \mathbf{0} \\ \mathbf{0} & \mathbf{0} & \mathbf{0} & \mathbf{0} & \mathbf{0} & \mathcal{A}_{\omega_3} & \mathbf{0} & \mathbf{0} & \mathbf{0} \\ \mathbf{0} & \mathbf{0} & \mathbf{0} & \mathbf{0} & \mathbf{0} & \mathbf{0} & \mathbf{0} & \mathbf{I}_8 & \mathbf{0} \\ \mathbf{0} & \mathbf{0} & \mathbf{0} & \mathbf{0} & \mathbf{0} & \mathbf{0} & \mathbf{0} & \mathbf{0} & \mathbf{I}_8 \\ \mathbf{0} & \mathbf{0} & \mathbf{0} & \mathbf{0} & \mathbf{0} & \mathbf{0} & \mathbf{0} & \mathbf{0} & \mathcal{A}_{\text{net}} \end{bmatrix}_{70 \times 70}$$

$$\mathbf{B} = [\mathbf{B}_1 \quad \mathbf{B}_2 \quad \mathbf{B}_3]_{70 \times 17}$$

where the blocks regarding $\mathcal{A}_{\text{inv}i}$ ($i = 1, \dots, 3$) at the upper-left of \mathbf{A} correspond to the linear parts of the inverter models; the blocks regarding $\mathcal{A}_i^{j,k}$ at the upper-middle of \mathbf{A} correspond to the linear part of DER output power and currents; the blocks regarding $\mathcal{A}_{\omega i}$ ($i = 1, \dots, 3$) at the middle of \mathbf{A} correspond to the nonlinear part of DER output power and currents; the blocks regarding \mathcal{A}_{net} and \mathbf{I} at the lower-right of \mathbf{A} correspond to the network topology. \mathbf{B} has a similar arrangement.

For simplification, we define the elements in \mathbf{A} and \mathbf{B} with MATLAB language (e.g., $\mathcal{A}_1(:, 2:3)$ means the second to the third columns of matrix \mathcal{A}_1 and “;” denotes line break) $\mathcal{A}_1^1 = [\mathbf{0}_{10 \times 1}, \mathcal{A}_1(:, 1), \mathbf{0}_{10 \times 4}]$, $\mathcal{A}_1^{2,3} = [\mathbf{0}_{10 \times 4}, \mathcal{A}_1(:, 2:3), \mathbf{0}_{10 \times 2}]$, $\mathcal{A}_2^1 = [\mathcal{A}_2(:, 1), \mathbf{0}_{9 \times 5}]$, $\mathcal{A}_2^{2,3} = [\mathcal{A}_2(:, 2:3), \mathbf{0}_{9 \times 4}]$, $\mathcal{A}_2^{4,5} = [\mathcal{A}_2(:, 4:5), \mathbf{0}_{9 \times 6}]$, $\mathcal{A}_3^1 = [\mathcal{A}_3(:, 1), \mathbf{0}_{9 \times 5}]$, $\mathcal{A}_3^{2,3} = [\mathcal{A}_3(:, 2:3), \mathbf{0}_{9 \times 4}]$, $\mathcal{A}_3^{4,5} = [\mathbf{0}_{9 \times 2}, \mathcal{A}_3(:, 4:5), \mathbf{0}_{9 \times 4}]$, $\mathbf{k}_i = [1, 0, K_{\text{pvi}0}, b_i]^T$ for $i = 1, 2, 3$. $\mathbf{B}_1 = [\mathbf{k}_1, \mathbf{0}_{1 \times 65}; \mathbf{0}_{1 \times 11}, \mathbf{k}_2, \mathbf{0}_{1 \times 54}; \mathbf{0}_{1 \times 20}, \mathbf{k}_3, \mathbf{0}_{1 \times 45}]^T$, $\mathbf{B}_2 = [\mathbf{0}_{2 \times 32}, \mathbf{I}_2, \mathbf{0}_{2 \times 36}; \mathbf{0}_{2 \times 38}, \mathbf{I}_2, \mathbf{0}_{2 \times 30}; \mathbf{0}_{2 \times 44}, \mathbf{I}_2, \mathbf{0}_{2 \times 24}]^T$, $\mathbf{B}_3 = [\mathbf{0}_{62 \times 8}; \mathbf{I}_8]$, and

$$\mathcal{A}_{\omega i} = \begin{bmatrix} 0 & 0 & 1 & 0 & 0 & 0 \\ 0 & 0 & 0 & 1 & 0 & 0 \\ 0 & 0 & 0 & 0 & 1 & 0 \\ 0 & 0 & 0 & 0 & 0 & 1 \\ 0 & 0 & 0 & 0 & -\omega_{ci} & 0 \\ 0 & 0 & 0 & 0 & 0 & -\omega_{ci} \end{bmatrix}$$

Remark 2: One of the benefits of model-based KO identification methods over data-driven ones is their scalability, which stems from the absence of data requirements. The proposed

analytical KO identification methodology has a modular design that facilitates the scaling up of the MG. This can be achieved by simply inserting additional block matrices at the appropriate locations in the KO-linearized system matrices \mathbf{A} and \mathbf{B} , and then adjusting the matrix \mathcal{A}_{net} to reflect the new network topology.

Remark 3: The purpose of the KO-linearized model (36) is to enable general linear control techniques that are still effective for the original nonlinear system. In practical application, the lifted-dimensional controller \mathbf{U} will be designed based on the auxiliary linear model (36) using any general linear control methods. Then, an analytical actual control signal \mathbf{u} will be obtained from \mathbf{U} . Finally, \mathbf{u} will be applied to the original nonlinear MG system (11). It should also be noted that since part of system dynamics $\mathbf{F}(\mathbf{x})$ is included in the control term $\mathbf{B}\mathbf{U}$, one should not expect stability of the original nonlinear model (11) can be analyzed through the eigenvalues of \mathbf{A} (assuming zero input) as usually done in small-signal models. This problem is further discussed in the case study section.

IV. VOLTAGE CONTROL OF MG BASED ON THE KO-LINEARIZED MODEL

A critical contribution of this work is that users can select any linear control methods according to their requirements on their control objectives. In this section, we use MG’s voltage restoration problem as an example to demonstrate how to use the above-developed linear MG model based on the KO theory. The control objective is to eliminate the steady-state errors between the output voltages of DERs and their reference values caused by the droop characteristics [2].

A. Controller Design Based on KO-Linearized Model With LQI

To achieve zero-offset voltage regulation and facilitate easy deployment, the optimal control method LQI is adopted in this Section [17].

Firstly, as shown in the very left block in Fig. 4, an integrator that dynamically feeds back the integral of the offset between DER output voltages and their references is designed as follows,

$$\dot{\mathbf{z}}_I = \mathbf{y}_{\text{ref}} - \mathbf{y}, \quad (37)$$

546 where \mathbf{z}_I denotes the error dynamics of the integrator and \mathbf{y}_{ref}
547 contains the voltage setpoints to be tracked.

548 Then, by defining new state vector $\tilde{\mathbf{z}} \triangleq [\mathbf{z}^\top - \mathbf{z}_\infty^\top, \mathbf{z}_I^\top]^\top$,
549 control input vector $\tilde{\mathbf{U}} = [\mathbf{U} - \mathbf{U}_\infty]$ and output offset vector
550 $\tilde{\mathbf{y}}(k) = \mathbf{y}(k) - \mathbf{y}_{\text{ref}}$, the bias system is derived as follows,

$$551 \quad \dot{\tilde{\mathbf{z}}} = \tilde{\mathbf{A}}\tilde{\mathbf{z}} + \tilde{\mathbf{B}}\tilde{\mathbf{U}}, \quad (38a)$$

$$552 \quad \tilde{\mathbf{y}} = \tilde{\mathbf{C}}\tilde{\mathbf{z}} \quad (38b)$$

553 where the system matrices of the above-augmented system are
554 given as

$$555 \quad \tilde{\mathbf{A}} = \begin{bmatrix} \mathbf{A} & \mathbf{0} \\ -\mathbf{C} & \mathbf{0} \end{bmatrix}, \tilde{\mathbf{B}} = \begin{bmatrix} \mathbf{B} \\ \mathbf{0} \end{bmatrix}, \tilde{\mathbf{C}} = [\mathbf{C} \quad \mathbf{0}]. \quad (39)$$

556 Finally, to achieve offset-free setpoint tracking, the steady-
557 state values \mathbf{z}_∞ and \mathbf{U}_∞ should satisfy

$$558 \quad \begin{bmatrix} \mathbf{A} & \mathbf{B} \\ \mathbf{C} & \mathbf{0} \end{bmatrix} \begin{bmatrix} \mathbf{z}_\infty \\ \mathbf{U}_\infty \end{bmatrix} = \begin{bmatrix} \mathbf{0} \\ \mathbf{y}_{\text{ref}} \end{bmatrix}. \quad (40)$$

559 Considering the following optimal performance index for
560 the continuous-time system (38),

$$561 \quad J = \frac{1}{2} \int_{t=0}^{\infty} (\tilde{\mathbf{z}}^\top \mathbf{Q} \tilde{\mathbf{z}} + \tilde{\mathbf{U}}^\top \mathbf{R} \tilde{\mathbf{U}}) dt, \quad (41)$$

562 where \mathbf{Q} and \mathbf{R} are weighting matrices. The optimal control
563 law minimizing J is derived as

$$564 \quad \tilde{\mathbf{U}} = -\mathbf{R}^{-1} \tilde{\mathbf{B}}^\top \mathbf{P} \tilde{\mathbf{z}}, \quad (42)$$

$$565 \quad \mathbf{U} = -\mathbf{R}^{-1} \tilde{\mathbf{B}}^\top \mathbf{P} \tilde{\mathbf{z}} + \mathbf{U}_\infty, \quad (43)$$

566 where \mathbf{P} is the unique positive definite solution to the following
567 continuous-time algebraic Riccati equation

$$568 \quad \tilde{\mathbf{A}}^\top \mathbf{P} + \mathbf{P} \tilde{\mathbf{A}} - \mathbf{P} \tilde{\mathbf{B}} \mathbf{R}^{-1} \tilde{\mathbf{B}}^\top \mathbf{P} + \mathbf{Q} = \mathbf{0}. \quad (44)$$

569 When the bias system (38)-(40) is stabilized by $\tilde{\mathbf{U}}$ in
570 Eq. (42), it is equivalent that: a) the KO-linearized model (36)
571 is stabilized; b) the DER output voltages of (36), \mathbf{y} is regulated
572 to the setpoint \mathbf{y}_{ref} with zero offsets, since $\dot{\mathbf{z}}_I = \mathbf{y}_{\text{ref}} - \mathbf{y} = \mathbf{0}$.

573 B. Recovering Lower-Dimensional Control Signal for the 574 Original MG System From the Lifted Control Vector

575 Note that the lifted control vector $\mathbf{U} \in \mathbb{R}^M$ of the KO-
576 linearized model (36) is of higher dimensional than the control
577 vector $\mathbf{u} \in \mathbb{R}^m$ of the original nonlinear MG model (11). Thus,
578 the lifted control signal \mathbf{U} is not directly applicable. Since the
579 first three elements of \mathbf{U} are just \mathbf{u} , one can use them as the
580 control inputs of the original MG system. However, such a
581 choice is no longer optimal due to the loss of information of
582 the other elements in \mathbf{U} . Therefore, we propose the following
583 optimal control signal recovery method.

584 Denote $\mathbf{U}_{\text{pq}} = [\mathbf{U}_{\text{pq}1}, \dots, \mathbf{U}_{\text{pq}m}]^\top$, $\mathcal{B}_{\text{pq}} =$
585 $[\mathcal{B}_{\text{pq}1}, \dots, \mathcal{B}_{\text{pq}m}]^\top$ and $\mathbf{f}_{\text{pq}} = [\mathbf{f}_{\text{pq}1}, \dots, \mathbf{f}_{\text{pq}m}]^\top$, from (24)
586 and (33), it has

$$587 \quad \begin{aligned} \mathbf{B}\mathbf{U} &= \mathbf{B}_1 \mathbf{u} + \mathbf{B}_2 \mathbf{U}_{\text{pq}} + \mathbf{B}_3 \mathbf{U}_{\text{net}} \\ &= \mathbf{B}_1 \mathbf{u} + \mathbf{B}_2 (\mathbf{f}_{\text{pq}}(\mathbf{x}) + \mathcal{B}_{\text{pq}} \mathbf{u}) + \mathbf{B}_3 (\mathbf{f}_{\text{net}}(\mathbf{x}) + \mathcal{B}_{\text{net}} \mathbf{u}) \\ &= \underbrace{\mathbf{B}_2 \mathbf{f}_{\text{pq}}(\mathbf{x}) + \mathbf{B}_3 \mathbf{f}_{\text{net}}(\mathbf{x})}_{\mathbf{F}(\mathbf{x})} + \underbrace{(\mathbf{B}_1 + \mathbf{B}_2 \mathcal{B}_{\text{pq}} + \mathbf{B}_3 \mathcal{B}_{\text{net}})}_{\mathcal{B}} \mathbf{u} \end{aligned} \quad (45)$$

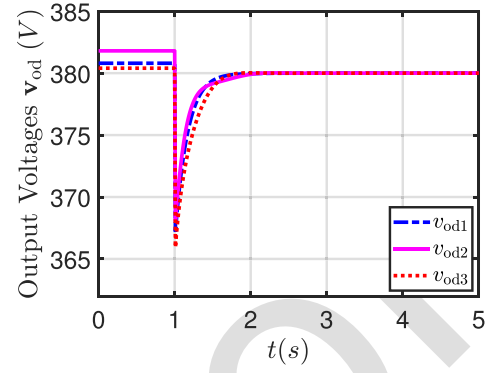


Fig. 5. Dynamic responses of DER output voltages of the test MG.

Notice that matrix \mathcal{B} is not a square matrix such that \mathbf{u} cannot
be directly retrieved via \mathcal{B}^{-1} . Therefore, we optimally recover
 \mathbf{u} from \mathbf{U} by solving the following least square problem,

$$594 \quad \min \frac{1}{2} (\mathcal{B}\mathbf{u} - (\mathbf{B}\mathbf{U} - \mathbf{F}(\mathbf{x})))^\top (\mathcal{B}\mathbf{u} - (\mathbf{B}\mathbf{U} - \mathbf{F}(\mathbf{x}))) \quad (46)$$

whose solution is

$$596 \quad \mathbf{u} = (\mathcal{B}^\top \mathcal{B})^{-1} \mathcal{B}^\top (\mathbf{B}\mathbf{U} - \mathbf{F}(\mathbf{x})). \quad (47)$$

By substituting (43) into (47), the controller for original
MG (11) is obtained as follows

$$599 \quad \mathbf{u} = (\mathcal{B}^\top \mathcal{B})^{-1} \mathcal{B}^\top (\mathbf{B}\mathbf{U}_\infty - \mathbf{B}\mathbf{R}^{-1} \tilde{\mathbf{B}}^\top \mathbf{P} \tilde{\mathbf{z}} - \mathbf{F}(\mathbf{x})) \quad (48)$$

Remark 4: The nonlinear term $\mathbf{F}(\mathbf{x})$ in the control law (48)
has a known expression that can be computed by inserting
the values of the state variables \mathbf{x} . Moreover, \mathbf{U}_∞ and \mathbf{z}_∞
are calculated through Eq. (40), \mathbf{z} in $\tilde{\mathbf{z}}$ can be substituted by
the designed measurement function $\mathbf{z} = \mathbf{g}(\mathbf{x}, \mathbf{u})$ and \mathbf{z}_I can
be directly obtained via the integrator (37). Thus, the controller (48)
only requires feedback of \mathbf{x} and is ready to be implemented in the original MG system (11).

The overall closed-loop MG control system based on the
KO and LQI is shown in Fig. 4.

610 V. CASE STUDIES

This section presents several case studies that demonstrate
the effectiveness of using the developed KO-linearized model
with the traditional LQI control method to stabilize the original
nonlinear MG system and eliminate the steady-state error of
DER output voltages caused by the droop equations.

616 A. Simulation Setup

The test system is a widely used 220 V MG with three
inverter-based DERs as shown in Fig. 3 [8]. The network
is resistance-dominated for such a low-voltage distribution
system. Table I provides the parameter setting and initial states
in this section. All three DERs are rated at 10 kVA with the
same droop gain, so the load consumption is shared equally.
Before the designed controller \mathbf{u} in (48) is applied, the voltage
setpoints $v_{\text{set}i}$ ($i = 1, \dots, 3$) in the droop equation (2b)
for each DER are set as 380 V, resulting in steady-state errors
in DER output voltages v_{odi} . All the dynamic simulations are

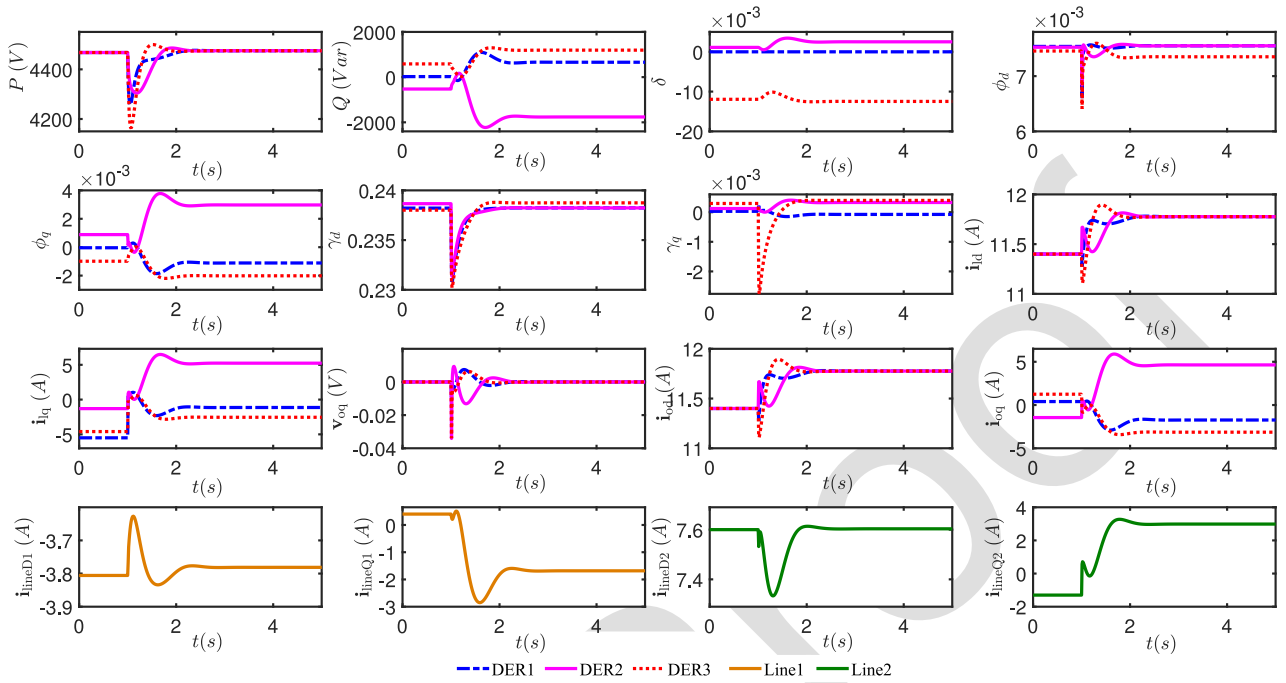


Fig. 6. Dynamic responses of all the other state variables of the test MG.

TABLE I
PARAMETER SETTING OF MG

	Par.	Value	Par.	Value
Initial	$v_{od}(0)$	[380.8, 381.8, 380.4]	$v_{oq}(0)$	[0, 0, 0]
	$i_{od}(0)$	[11.4, 11.4, 11.4]	$i_{oq}(0)$	[0.4, -1.45, 1.25]
	$i_{id}(0)$	[11.4, 11.4, 11.4]	$i_{iq}(0)$	[-5.5, -7.3, -4.6]
	$\omega(0)$	314	δ_0	[0, 0.0019, -0.0113]
	$i_{line1d}(0)$	-3.8	$i_{line1q}(0)$	0.4
	$i_{line2d}(0)$	7.6	$i_{line2q}(0)$	-1.3
Line and	r_{line1}	0.23 Ω	x_{line1}	0.1 Ω
	r_{line2}	0.35 Ω	x_{line2}	0.58 Ω
Load	r_{load1}	25 Ω	x_{load3}	20 Ω
DER	The DER parameters can be found in [8]			

627 conducted in the MATLAB environment on a standard PC with
628 an Intel Core i9-13900HX CPU running at 2.20 GHz and with
629 32.0 GB of RAM.

630 B. Control Performance Based on the KO and LQI

631 The proposed KO-linearized MG model for the voltage control of MGS is verified by applying the LQI controller (48) to
632 the original nonlinear MG model (11) after 1 s. Before that, the
633 voltage setpoints for the droop equations are kept constant at
634 $\mathbf{u} = [380, 380, 380]^T$ V. Figure 5 shows that the DER output
635 voltages have steady-state errors due to the droop characteristic
636 before 1 s. When the proposed KO-based LQI controller takes
637 over, the steady-state errors are quickly eliminated, confirming
638 the effectiveness of the proposed method.

639 Figure 6 shows the dynamic responses of all the other stable
640 variables. It can be observed that all the state variables are

642 stabilized to a new equilibrium point. For a more systematic
643 study of the system stability, we compare the poles of the
644 system (36) before and after the LQI controller $\tilde{\mathbf{U}}$ are applied,
645 i.e., eigenvalues of \mathbf{A} and $\tilde{\mathbf{A}} - \tilde{\mathbf{B}}\mathbf{K}$. The maximum of the real
646 part of eigenvalues of matrix \mathbf{A} is 7.7709×10^{-11} while that
647 of matrix $\tilde{\mathbf{A}} - \tilde{\mathbf{B}}\mathbf{K}$ is -9.4000×10^{-4} . However, it should be
648 mentioned that the original nonlinear system (11) is actually
649 stable with the provided configuration. The reason that the KO-
650 linearized model (36) has positive poles (indicating unstable
651 modes) is that part of system dynamics $\mathbf{F}(\mathbf{x})$ is absorbed into
652 the term $\mathbf{B}\mathbf{U}$ as discussed in Remark 1. Therefore, the poles
653 of \mathbf{A} only reflect the open-loop stability of the KO-linearized
654 system (36), but do not indicate the stability of the original
655 nonlinear system (11). With the application of LQI, all the
656 poles are placed on the plane's left side, indicating that the
657 LQI controller stabilizes the system (36) as shown in Fig. 7.

658 The lifted control vector \mathbf{U} can stabilize the MG system as
659 verified by the above pole analysis. However, the proposed
660 KO-based control scheme also relies on the approximation
661 of the original control input \mathbf{u} by solving the least square
662 optimization problem (46), which introduces an approxima-
663 tion error. Figure 8 shows that the least square approximation
664 error converges to a small value of 0.124 after 4 s, implying
665 that the approximation error has a negligible impact on the
666 overall control performance in this case.

667 C. Model Error and Sensitivity Analyses

668 The KO-linearized model (36) is derived analytically, so
669 the only source of model error between (36) and (11) should
670 be the assumptions made in the model development, namely
671 $\sin \delta_i \approx \delta_i$, $\cos \delta_i \approx 1$, and $\omega_i \approx \omega_n$ in the LC filters and
672 lines. To verify this claim, we set $\mathbf{u} = [380, 380, 380]^T$ V for

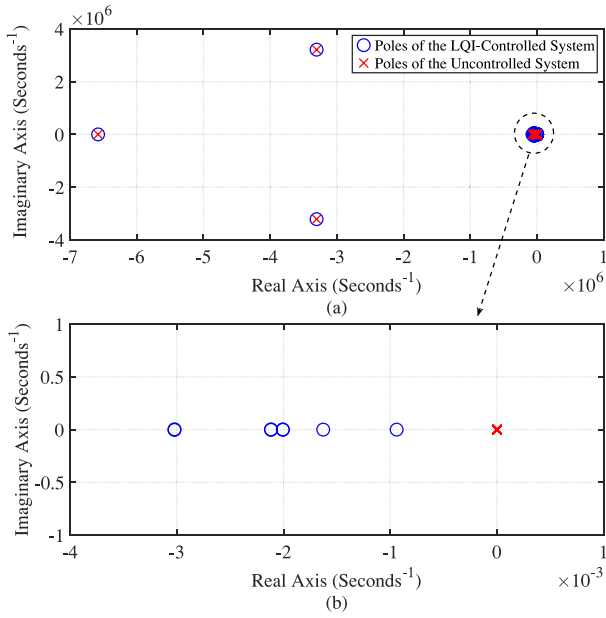


Fig. 7. Comparison of poles of system (36) before and after the LQI controller \mathbf{U} is applied.

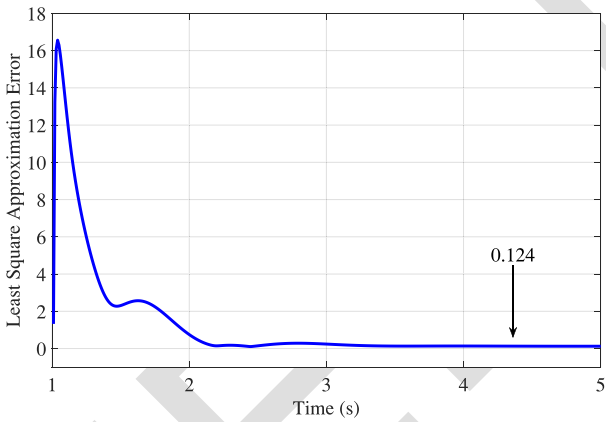


Fig. 8. The time-varying approximation error of the control signal using the least square method (46).

both (11) and (36). Since the observable vector \mathbf{z} contains an explicit representation of the state vector of the original MG \mathbf{x} , we can denote the \mathbf{x} in \mathbf{z} as \mathbf{z}_x . This allows us to directly compare the dynamic responses of the two models. Use mean absolute error (MAE) to define the model error as

$$\text{MAE}(t) = \frac{1}{n} \sum_{i=1}^n |\mathbf{x}(t) - \mathbf{z}_x(t)|. \quad (49)$$

We also conduct sensitivity analysis of the developed KO-linearized model by simulating 50 different sets of initial conditions. For each run, we add a 30% random perturbation to the initial condition in Table I. Figure 9 shows that all the model errors $\text{MAE}(t)$ with different initial conditions oscillate late during the settling period and finally converge to around 0.357. Moreover, the $\text{MAE}(t)$ is always below 1 throughout the timeline. To investigate the source of the steady-state error, we examine the detailed error of each state. Figure 10 reveals that the steady-state errors mainly occur in the active and reactive powers, but their actual values are negligible compared

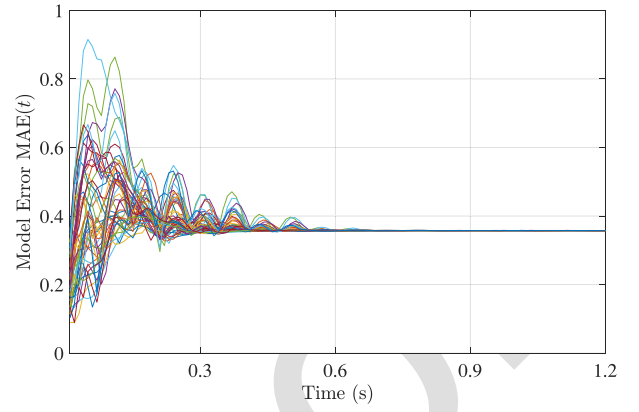


Fig. 9. The time-varying model error measured by MAE with 50 different initial condition settings.

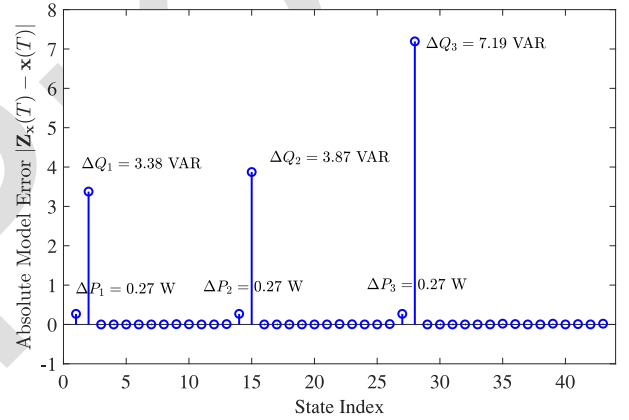


Fig. 10. The steady-state absolute model error of each state at time $T = 5$ seconds. ΔP and ΔQ denote the absolute error of real and reactive powers, respectively.

to the magnitude of P and Q . Therefore, we conclude that the developed KO-linearized model is sufficiently accurate and robust against different initial conditions.

D. Comparison Case Studies

This subsection compares the proposed LQI control method based on the KO-linearized model with two common MG voltage control methods. The first method is a proportional-integral-derivative (PID) control based on the original nonlinear MG model (11), with the output function $\mathbf{y} = [v_{od1}, v_{od2}, v_{od3}]$. The proportional, integral, and derivative gains for all three PID controllers are set to 1.5, 320, and 0, respectively. The second method is an LQI control based on the small-signal model (first-order Taylor expansion) from [8], with the same LQI setting as in Section V-B.

As shown in Fig. 11, the PID and SS+LQI achieve significantly faster dynamic response speeds than the KO+LQI. However, they also lead to much larger overshoots during the transients, which are hazardous for MG operation. Furthermore, the comparison between SS+LQI and KO+LQI reveals that the proposed KO-linearized model can capture the nonlinear dynamics more precisely than the small-signal model based on first-order Taylor expansion, resulting in a smoother dynamic performance.

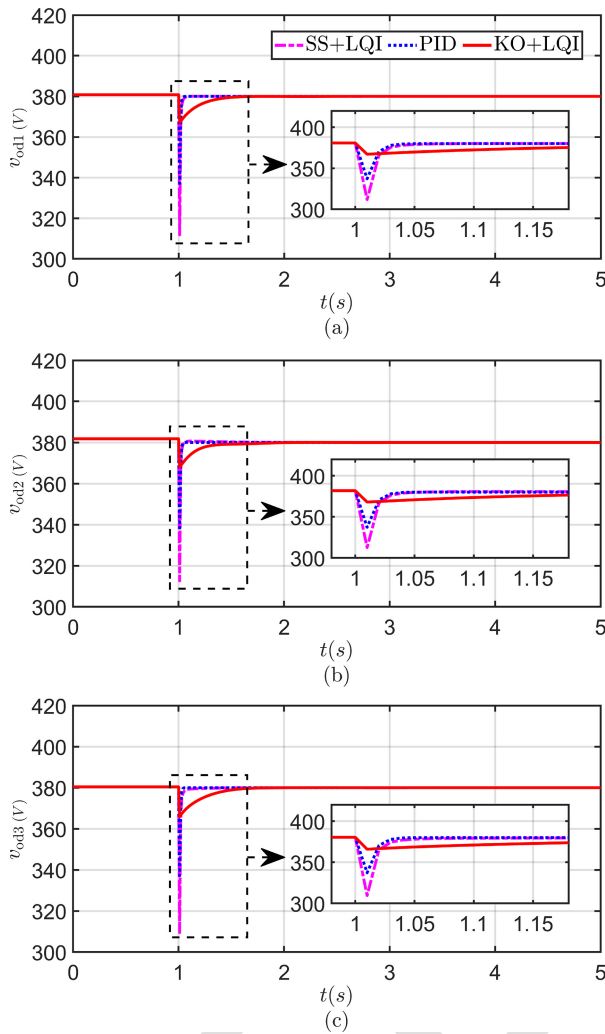


Fig. 11. Comparison of the control performances of DER output voltages using the small-signal-model-based LQI (SS+LQI), original-nonlinear-model-based PID, and the proposed KO-linearized-model-based LQI (KO+LQI).

E. Computational Efficiency Analysis

The performance of the KO-based method in terms of computational efficiency can be evaluated by considering two aspects: the identification of KO and the dynamic simulation of the controlled MG system.

Firstly, the proposed KO identification method is fully model-based which means the analytical linear system (36) is manually derived offline. Therefore, the proposed analytical KO derivation approach does not require any computational effort. This contrasts with the data-driven methods that rely on numerical computation of the KO [20], [21], [22], [23], [24], [25], [26].

The second aspect of the computational efficiency of the KO-based method is the impact of the increased dimension of the studied MG system, which is lifted from 43 to 70 in this case. To assess this impact, we compare the computational times of dynamic simulations of the proposed KO+LQI method with the two other methods (based on unlifted-dimensional MG models) studied in Section V-D. The simulation is performed using the ode15s solver with

0.01 s sampling time over 5 s dynamic simulation duration in MATLAB. The average computational times over 100 runs of PID, SS+LQI, and the proposed KO+LQI methods are 0.0218 s, 0.0232 s, and 0.0422 s, respectively. We can see that, the computational times of PID and SS+LQI are similar because they both use the original 43-dimensional MG system. On the other hand, the computational time of the proposed KO+LQI method is higher than the others mainly due to the increased system dimension, however, it is still sufficiently fast for practical implementation.

VI. CONCLUSION

This paper presents a novel large-signal method to linearize microgrid (MG) models for controller design using the Koopman operator (KO) theory. The primary and zero control levels are modeled for electromagnetic transient (EMT) analysis, which increases system order and nonlinearity. To overcome these challenges, we have derived the observable functions and KO analytically, avoiding data dependence and improving explainability. Voltage control with linear quadratic integrator (LQI) is used as an example to show how our KO-linearized model enables textbook linear control techniques for nonlinear MGS. To guarantee stabilizability, a lifted-dimensional control signal has been derived in the KO-linearized model. We use least squares to map the high-dimensional control vector to the original one. The case studies validate the LQI and KO-linearized model for DER output voltage restoration. The model error without a state-feedback controller under different initial conditions confirms the accuracy and robustness of our analytical KO-linearized MG model. Comparison case studies with benchmark approaches such as PID and small-signal-model-based methods are conducted to validate the advantages of the proposed KO-based MG voltage control scheme. The proposed analytical derivation methodology is generic and applicable to other MG systems with different structures and objectives due to a modular design.

Our future work will focus on discovering the theoretical stability analysis of the original nonlinear system (11), i.e., developing a sufficient condition with respect to \mathbf{A} , \mathbf{B} , $\mathbf{F}(\mathbf{x})$ and \mathbf{B} , under which, the control signal \mathbf{u} recovered by the least square method can *theoretically* ensure the stability of the original system (11). This mathematical problem is still fundamentally challenging, but its solution can contribute to addressing a wide class of nonlinear control problems.

REFERENCES

- J. C. Vasquez, J. M. Guerrero, J. Miret, M. Castilla, and L. G. de Vicuña, "Hierarchical control of intelligent microgrids," *IEEE Ind. Electron. Mag.*, vol. 4, no. 4, pp. 23–29, Dec. 2010.
- A. Bidram and A. Davoudi, "Hierarchical structure of microgrids control system," *IEEE Trans. Smart Grid*, vol. 3, no. 4, pp. 1963–1976, Dec. 2012.
- Q. Zhang, Z. Ma, Y. Zhu, and Z. Wang, "A two-level simulation-assisted sequential distribution system restoration model with frequency dynamics constraints," *IEEE Trans. Smart Grid*, vol. 12, no. 5, pp. 3835–3846, Sep. 2021.
- Z. Ma, Z. Wang, Y. Guo, Y. Yuan, and H. Chen, "Nonlinear multiple models adaptive secondary voltage control of microgrids," *IEEE Trans. Smart Grid*, vol. 12, no. 1, pp. 227–238, Jan. 2021.

- [5] R. Cheng, N. Shi, S. Maharjan, and Z. Wang, "Automatic self-adaptive local voltage control under limited reactive power," *IEEE Trans. Smart Grid*, vol. 14, no. 4, pp. 2851–2862, Jul. 2023.
- [6] B. Chen, J. Wang, X. Lu, C. Chen, and S. Zhao, "Networked microgrids for grid resilience, robustness, and efficiency: A review," *IEEE Trans. Smart Grid*, vol. 12, no. 1, pp. 18–32, Jan. 2021.
- [7] W. Cui, Y. Jiang, and B. Zhang, "Reinforcement learning for optimal primary frequency control: A Lyapunov approach," *IEEE Trans. Power Syst.*, vol. 38, no. 2, pp. 1676–1688, Mar. 2023.
- [8] N. Pogaku, M. Prodanovic, and T. C. Green, "Modeling, analysis and testing of autonomous operation of an inverter-based microgrid," *IEEE Trans. Power Electron.*, vol. 22, no. 2, pp. 613–625, Mar. 2007.
- [9] M. Rasheduzzaman, J. A. Mueller, and J. W. Kimball, "An accurate small-signal model of inverter-dominated islanded microgrids using dq reference frame," *IEEE J. Emerg. Sel. Top. Power Electron.*, vol. 2, no. 4, pp. 1070–1080, Dec. 2014.
- [10] Q. Shafiee, Č. Stefanović, T. Dragičević, P. Popovski, J. C. Vasquez, and J. M. Guerrero, "Robust networked control scheme for distributed secondary control of islanded microgrids," *IEEE Trans. Ind. Electron.*, vol. 61, no. 10, pp. 5363–5374, Oct. 2014.
- [11] A. Bidram, A. Davoudi, F. L. Lewis, and J. M. Guerrero, "Distributed cooperative secondary control of microgrids using feedback linearization," *IEEE Trans. Power Syst.*, vol. 28, no. 3, pp. 3462–3470, Aug. 2013.
- [12] A. Bidram, F. L. Lewis, and A. Davoudi, "Distributed control systems for small-scale power networks: Using multiagent cooperative control theory," *IEEE Control Syst. Mag.*, vol. 34, no. 6, pp. 56–77, Dec. 2014.
- [13] Y. Du, X. Lu, B. Chen, and F. Lin, "Resiliency augmented hybrid AC and DC distribution systems with inverter-dominated dynamic microgrids," *IEEE Trans. Smart Grid*, vol. 13, no. 5, pp. 4088–4101, Sep. 2022.
- [14] J. Lai, X. Lu, and X. Yu, "Stochastic distributed frequency and load sharing control for microgrids with communication delays," *IEEE Syst. J.*, vol. 13, no. 4, pp. 4269–4280, Dec. 2019.
- [15] J. Lai, X. Lu, X. Yu, and A. Monti, "Stochastic distributed secondary control for AC microgrids via event-triggered communication," *IEEE Trans. Smart Grid*, vol. 11, no. 4, pp. 2746–2759, Jul. 2020.
- [16] A. Maulik and D. Das, "Stability constrained economic operation of islanded droop-controlled dc microgrids," *IEEE Trans. Sustain. Energy*, vol. 10, no. 2, pp. 569–578, Apr. 2019.
- [17] Z. Ma, Q. Zhang, and Z. Wang, "Safe and stable secondary voltage control of microgrids based on explicit neural networks," *IEEE Trans. Smart Grid*, vol. 14, no. 5, pp. 3375–3387, Sep. 2023, doi: [10.1109/TSG.2023.3239548](https://doi.org/10.1109/TSG.2023.3239548).
- [18] B. O. Koopman, "Hamiltonian systems and transformation in Hilbert space," *Proc. Nat. Acad. Sci.*, vol. 17, no. 5, pp. 315–318, Mar. 1931.
- [19] J. Yao, Q. Hu, and J. Zheng, "Koopman-operator-based safe learning control for spacecraft attitude reorientation with angular velocity constraints," *IEEE Trans. Aerosp. Electron. Syst.*, early access, Jun. 13, 2023, doi: [10.1109/TAES.2023.3285725](https://doi.org/10.1109/TAES.2023.3285725).
- [20] A. E. Saldaña, E. Barocio, A. R. Messina, J. J. Ramos, R. J. Segundo, and G. A. Tinajero, "Monitoring harmonic distortion in microgrids using dynamic mode decomposition," in *Proc. IEEE Power Energy Soc. Gen. Meeting*, 2017, pp. 1–5.
- [21] G. Kandaperumal, K. P. Schneider, and A. K. Srivastava, "A data-driven algorithm for enabling delay tolerance in resilient microgrid controls using dynamic mode decomposition," *IEEE Trans. Smart Grid*, vol. 13, no. 4, pp. 2500–2510, Jul. 2022.
- [22] M. O. Williams, I. G. Kevrekidis, and C. W. Rowley, "A data-driven approximation of the Koopman operator: Extending dynamic mode decomposition," *J. Nonlinear Sci.*, vol. 25, pp. 1307–1346, Jun. 2015.
- [23] M. Korda and I. Mezić, "Linear predictors for nonlinear dynamical systems: Koopman operator meets model predictive control," *Automatica*, vol. 93, pp. 149–160, Jul. 2018.
- [24] V. Toro, D. Tellez-Castro, E. Mojica-Nava, and N. Rakoto-Ravalontsalama, "Data-driven distributed voltage control for microgrids: A Koopman-based approach," *Int. J. Electr. Power Energy Syst.*, vol. 145, Feb. 2023, Art. no. 108636.
- [25] X. Gong, X. Wang, and G. Joos, "An online data-driven method for microgrid secondary voltage and frequency control with ensemble Koopman modeling," *IEEE Trans. Smart Grid*, vol. 14, no. 1, pp. 68–81, Jan. 2023.
- [26] X. Gong and X. Wang, "A novel Koopman-inspired method for the secondary control of microgrids with grid-forming and grid-following sources," *Appl. Energy*, vol. 333, Mar. 2023, Art. no. 120631.
- [27] S. Servadio, D. Arnas, and R. Linares, "Dynamics near the three-body libration points via Koopman operator theory," *J. Guid. Control Dyn.*, vol. 45, no. 10, pp. 1800–1814, Jul. 2022.
- [28] T. Chen and J. Shan, "Koopman-operator-based attitude dynamics and control on $SO(3)$," *J. Guid. Control Dyn.*, vol. 43, no. 11, pp. 2112–2126, Nov. 2020.
- [29] D. Arnas and R. Linares, "Approximate analytical solution to the zonal harmonics problem using Koopman operator theory," *J. Guid. Control Dyn.*, vol. 44, no. 11, pp. 1909–1923, Aug. 2021.
- [30] H. K. Khalil, *Nonlinear Systems*. Hoboken, NJ, USA: Prentice Hall, 2000.



Zixiao Ma (Member, IEEE) received the B.S. degree in automation and the M.S. degree in control theory and control engineering from Northeastern University, Shenyang, China, in 2014 and 2017, respectively, and the Ph.D. degree in electrical and computer engineering from Iowa State University, Ames, IA, USA, in 2023. He is currently a Postdoctoral Scholar with the Clean Energy Institute and the Department of Electrical and Computer Engineering, University of Washington, Seattle, WA, USA. His research interests focus on control theory and machine learning with their applications to inverter-based resources, microgrids, and load modeling. He was the recipient of the Outstanding Reviewer Award from IEEE TRANSACTIONS ON POWER SYSTEMS, the Research Excellence Award from Iowa State University, the Chinese Government Award for Outstanding Self-Financed Students Abroad, and the Distinguished Postdoctoral Fellowship from the University of Washington.



Zhaoyu Wang (Senior Member, IEEE) received the B.S. and first M.S. degrees in electrical engineering from Shanghai Jiao Tong University, and the second M.S. and Ph.D. degrees in electrical and computer engineering from the Georgia Institute of Technology. He is the Northrop Grumman Endowed Associate Professor with Iowa State University. His research interests include optimization and data analytics in power distribution systems and microgrids. He was the recipient of the National Science Foundation CAREER Award, the Society-Level Outstanding Young Engineer Award from IEEE Power and Energy Society, the Northrop Grumman Endowment, the College of Engineering's Early Achievement in Research Award, and the Harpole-Pentair Young Faculty Award Endowment. He is a Principal Investigator for a multitude of projects funded by the National Science Foundation, the Department of Energy, National Laboratories, PSERC, and Iowa Economic Development Authority. He is the Technical Committee Program Chair of IEEE Power System Operation, Planning and Economics Committee, the Chair of IEEE PSoPE Award Subcommittee, the Vice Chair of IEEE Distribution System Operation and Planning Subcommittee, and the Vice Chair of IEEE Task Force on Advances in Natural Disaster Mitigation Methods. He is an Associate Editor of IEEE TRANSACTIONS ON SUSTAINABLE ENERGY, IEEE OPEN ACCESS JOURNAL OF POWER AND ENERGY, IEEE POWER ENGINEERING LETTERS, and *IET Smart Grid*. He was an Associate Editor of IEEE TRANSACTIONS ON POWER SYSTEMS and IEEE TRANSACTIONS ON SMART GRID.



Rui Cheng (Member, IEEE) received the Ph.D. degree in electrical engineering from Iowa State University in 2023. He is currently an Assistant Professor with North China Electric Power University. His research interests include power distribution systems, voltage/var control, transactive energy markets, power system reliability and resilience, and applications of optimization and machine learning methods to power systems. He was the recipient of the Best Paper Award from the 2023 IEEE Power and Energy Society General Meeting, and the Research Excellence Award from Iowa State University.